Mechanical properties of Li–Sn alloys for Li-ion battery anodes: A first-principles perspective

Panpan Zhang, Zengsheng Ma, Wenjuan Jiang, Yan Wang, Yong Pan, and Chunsheng Lu

Citation: AIP Advances **6**, 015107 (2016); doi: 10.1063/1.4940131
View online: http://dx.doi.org/10.1063/1.4940131
View Table of Contents: http://scitation.aip.org/content/aip/journal/adva/6/1?ver=pdfcov
Published by the AIP Publishing

Mechanical properties of Li–Sn alloys for Li-ion battery anodes: A first-principles perspective

Panpan Zhang,[1] Zengsheng Ma,[1,a] Wenjuan Jiang,[1] Yan Wang,[2] Yong Pan,[1] and Chunsheng Lu[3,b]

[1]*National–Provincial Laboratory of Special Function Thin Film Materials, and School of Materials Science and Engineering, Xiangtan University, Xiangtan 411105, Hunan, China*
[2]*School of Information and Electronic Engineering, Hunan University of Science and Technology, Xiangtan 411201, Hunan, China*
[3]*Department of Mechanical Engineering, Curtin University, Perth, Western Australia 6845, Australia*

(Received 10 November 2015; accepted 5 January 2016; published online 13 January 2016)

Fracture and pulverization induced by large stress during charging and discharging may lead to the loss of electrical contact and capacity fading in Sn anode materials. A good understanding of mechanical properties is necessary for their optimal design under different lithiation states. On the basis of first-principles calculations, we investigate the stress-strain relationships of Li–Sn alloys under tension. The results show that the ideal tensile strengths of Li–Sn alloys vary as a function of Li concentration, and with the increase of Li^+ concentration, the lowest tensile strength decreases from 4.51 GPa (Sn) to 1.27 GPa (Li_7Sn_2). This implies that lithiation weakens the fracture resistance of Li–Sn alloys. [http://dx.doi.org/10.1063/1.4940131]

I. INTRODUCTION

As a promising anode material for Li-ion batteries (LIBs), Sn has attracted considerable interest due to its extremely high specific capacity of 994 mAh g^{-1}, which is much higher than that of graphite (372 mAh g^{-1}).[1–4] However, Sn anodes seriously suffer from repeated large compressive and tensile stresses during the battery cycles.[5,6] Unevenly distributed stress and nonuniform volume change in electrode materials lead to fracture and pulverization, causing the loss of electrical contact and capacity.[6] To overcome such a problem and realize optimal design of Sn anode materials, it is crucial to understand their mechanical properties in different lithiation states during charging and discharging processes. A number of experimental and theoretical works have been made on mechanical properties of Sn anode materials,[6–10] however, they are primarily concentrated on elastic properties. There are few studies on mechanical properties in large and inelastic strain approaching to fracture. In this letter, first-principles calculations are made to obtain ideal tensile strengths and stress-strain relationships of Li–Sn alloys. Here, the ideal tensile strength of a dislocation-free crystal is defined as the peak stress in a stress-strain curve along the weakest tensile stretch direction.[11] Also the evolution of microstructures is investigated for Sn anode materials under different Li-ion concentrations.

II. CALCULATION METHODOLOGY

The first-principles calculations have been carried out by using the VASP code,[12] with the local density approximation for exchange and correction functional.[13] To describe the ion-electron interaction, the projected augmented wave method is applied,[14] and the valence configurations of Li and Sn

[a]Corresponding author: zsma@xtu.edu.cn (Zengsheng Ma)
[b]Corresponding author: c.lu@curtin.edu.au (Chunsheng Lu)

TABLE I. Lattice constants (in the unit of Å) and k-points used in first-principles calculations, where y is the ratio of Li atoms (x) to the total number of atoms in Li_xSn alloys and experimental values are given in parentheses.

Phase	Space group	x	$y = x/(1+x)$	a	b	c	Volume	k-points
β-Sn	$I4_1/amd$	0.00	0.000	5.792 (5.831)	5.792 (5.831)	3.122 (3.184)[18]	104.78	9×9×16
Li_2Sn_5	$P4/mbm$	0.40	0.286	10.331 (10.274)	10.331 (10.274)	3.169 (3.125)[19]	338.20	3×3×11
LiSn	$P2/m$	1.00	0.500	5.162 (5.172)	7.764 (7.742)	3.233 (3.182)[20]	125.00	7×10×4
Li_7Sn_3	$P2_1/m$	2.33	0.700	9.495 (9.451)	8.536 (8.561)	4.738 (4.721)[21]	369.00	4×7×4
Li_5Sn_2	$R\bar{3}m$	2.50	0.714	4.725 (4.740)	4.725 (4.740)	19.844 (19.833)[22]	383.75	8×8×2
$Li_{13}Sn_5$	$P\bar{3}m1$	2.60	0.722	4.703 (4.701)	4.703 (4.701)	17.130 (17.124)[23]	328.14	8×8×2
Li_7Sn_2	$Cmmm$	3.50	0.778	9.847 (9.802)	13.838 (13.803)	4.712 (4.752)[24]	642.00	3×2×7
$Li_{17}Sn_4$	$F\bar{4}3m$	4.25	0.810	19.668 (19.691)	19.668 (19.691)	19.668 (19.691)[25]	7608.27	2×2×2
Li	Im3m	∞	1	3.436(3.513)	3.436(3.513)	3.436(3.513)[26]	40.58	22×22×22

are $1s^22s^1$ and $5s^25p^2$ ($4d^{10}$), respectively. The energy cutoff for a plane wave basis set is 500 eV and the Brillouin zone is sampled with the Monkhorst-Pack k-point grid (see Table I).[15] In calculations, all atoms are fully relaxed by the conjugate gradient method until residual forces on constituent atoms are less than 1×10^{-3} eV/Å. After obtaining the equilibrium structure, stress-strain relationships are determined by incrementally deforming lattice vectors in the applied strain direction. At each step, the applied tensile strain is fixed, while the atomic basis vectors orthogonal to strain and atoms inside the unit cell are simultaneously relaxed. To ensure a continuous strain path, the initial position is taken from the relaxed coordinates of a previous strain step.

III. RESULTS AND DISCUSSION

In first-principles calculations, a structure is firstly optimized to determine the lattice parameters and positions of atoms. For crystalline Li–Sn phases, their optimized structures are illustrated in insets of Fig. 1, and as listed in Table I, the results are in good agreement with available experimental data.

Based on these equilibrium structures, the stress-strain relationships of crystalline Li–Sn alloys are calculated under tension (see Fig. 1). As shown in Fig. 1(a), Sn with a tetragonal structure has strong stress responses in the [100], [001], [110], [011], and [111] directions, with the peak tensile stress between 4 and 10 GPa. Similarly, the peak tensile stress of Li_2Sn_5 with a tetragonal structure (see Fig. 1(b)) is between 2 and 7 GPa. For Sn, the highest peak tensile stress of 9.94 GPa is along the [100] direction, which is more than that of Li_2Sn_5 (6.15 GPa) in the [001] direction. In addition, the lowest peak stress of Sn (4.51 GPa at the strain of 0.12) along the [111] direction is also higher than that of Li_2Sn_5 (2.85 GPa at the strain of 0.16) in the [100] direction, indicating that a continuous lithiation process leads to significant bond weakening. Here, it is worth noting the maximum stress appears in the [100] direction for Sn, but in the case of Li_2Sn_5, it is just the opposite. Such a conversion is attributed to their structures such as different bond orientations and angles on the surface of (001), as shown in Figs. 1(a) and 1(b).

In the case of monoclinic LiSn and Li_7Sn_3 phases, their stress-strain curves in the [100], [010], and [001] directions are given in Figs. 1(c) and 1(d). It is found out that the weakest tensile strength of LiSn at a strain of 0.05 in the [010] direction is higher than that of Li_7Sn_3 at a strain of 0.03 in the [001] direction. However, Li_7Sn_3 achieves a second tensile strength peak of 3.72 GPa in the [001] direction, which is nearly 2 times the former. This is due to the strain dependence on their bond lengths and angles. It is obvious in Fig. 1(d) that both the angle (θ) between bonds 1 and 2 and the length of bond 2 increase with strain (see Fig. 2). The length of bond 1 firstly increases with the increase of strain, and then it decreases at the strain level larger than 0.14. However, a sudden increase of the bond angle θ occurs at a strain of 0.04 (see Fig. 2(a)), which leads to the first peak of tensile strength. The variation of θ also results in small fluctuations of the length of bond 1 at a strain of 0.04 (see Fig. 2(b)). The increase of the length of bond 2 is due to its stretch in the [001] direction. At a strain of 0.27, the length of bond 2 has a maximum value of 0.321 nm and the strength reaches the second peak. Then, the length of bond 2 abruptly changes at a strain of 0.28 (Fig. 2(b)), indicating that the bond 2 breaks. The bond breakage leads to a decrease of the tensile strength.

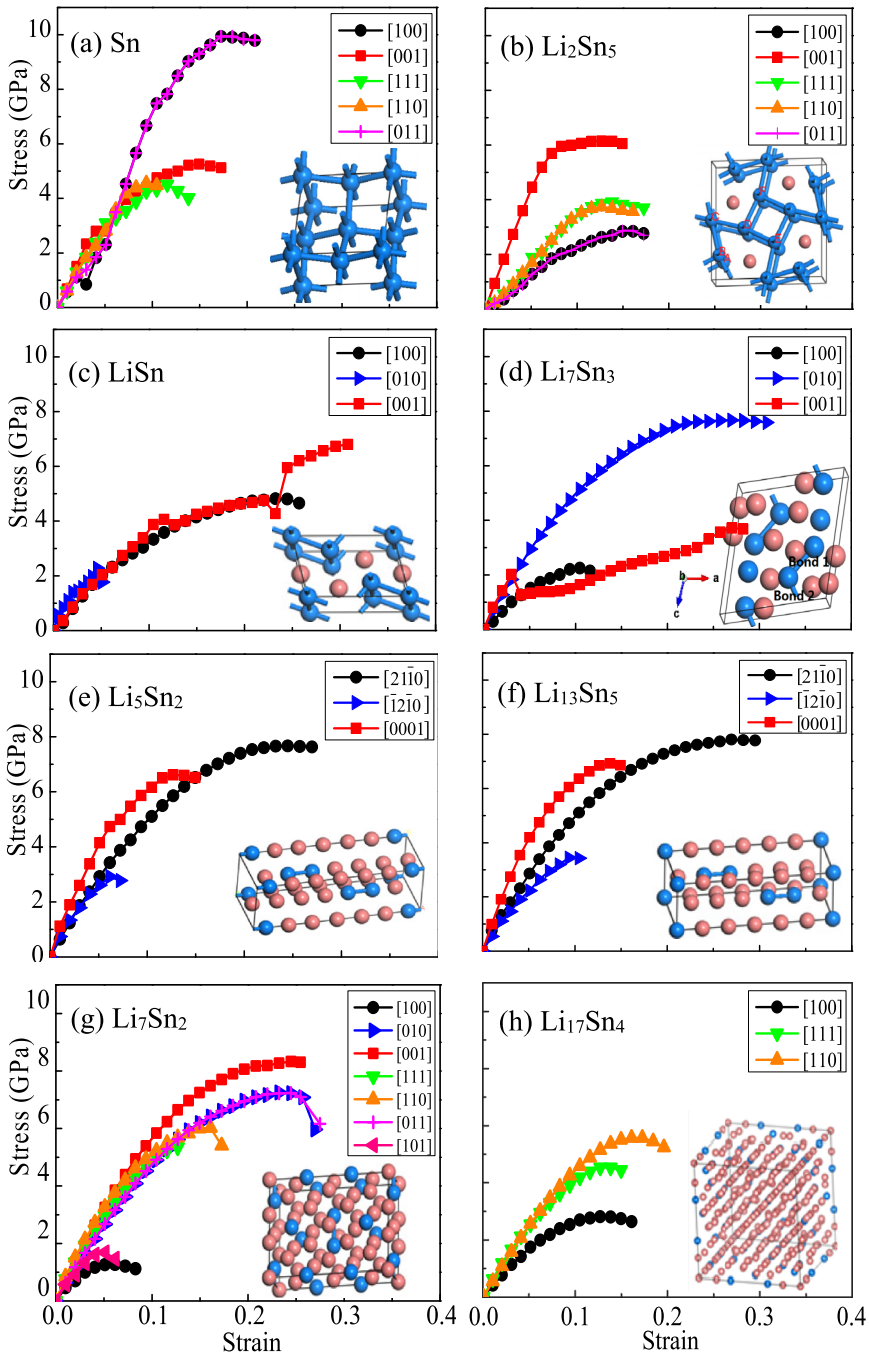

FIG. 1. The calculated stress-strain curves of Li–Sn alloys under tension, where insets show their crystalline structures.

In the case of hexagonal Li_5Sn_2 and $Li_{13}Sn_5$ phases, their ideal strengths are calculated along three principal symmetry crystallographic directions. As shown in Figs. 1(e) and 1(f), the ideal tensile strengths of Li_5Sn_2 are 7.67, 6.62, and 2.92 GPa in the $[21\bar{1}0]$, [0001], and $[\bar{1}2\bar{1}0]$ directions. The corresponding strengths of $Li_{13}Sn_5$ are 7.81, 6.92 and 3.44 GPa, respectively. Hence, it is seen that Li_5Sn_2 and $Li_{13}Sn_5$ have similar highest and lowest tensile strengths. In addition, the anisotropy ratios of $[21\bar{1}0]$:[0001]:$[\bar{1}2\bar{1}0]$ for Li_5Sn_2 and $Li_{13}Sn_5$ are 2.63:2.27:1 and 2.27:2.01:1, respectively. These results are consistent to their linear elastic properties,[7] because of their similar structures and almost the same number of Li–Sn and Li–Li chemical bonds (see insets in Figs. 1(e) and 1(f)).

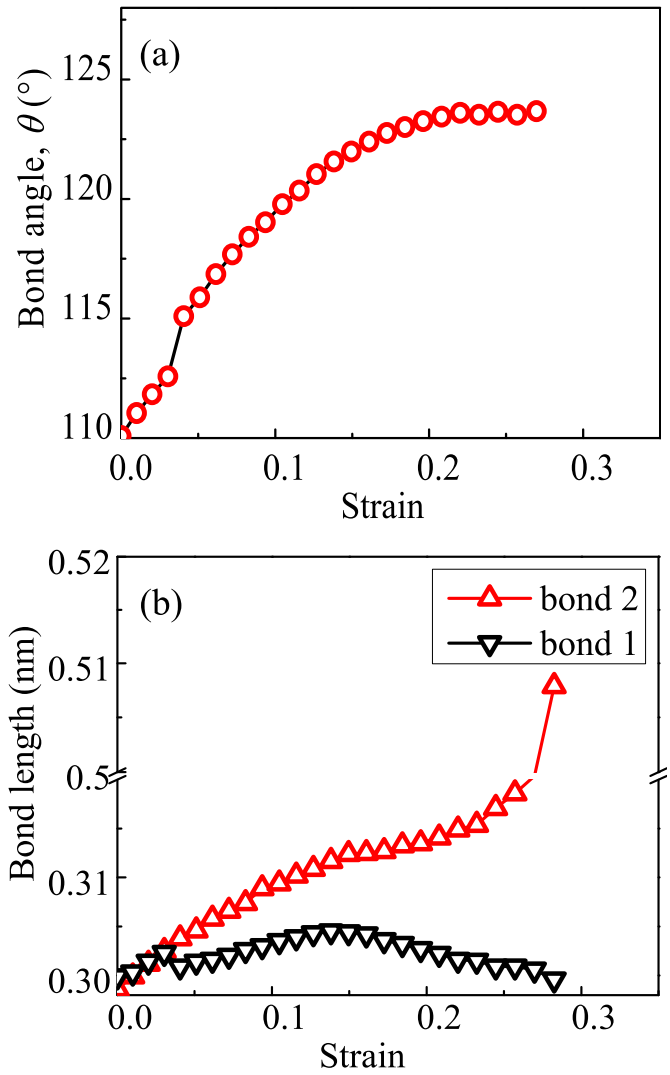

FIG. 2. Dependence of (a) the angle θ between bonds 1 and 2 and (b) their bond lengths in Li_7Sn_3 (see inset in Fig. 1(d)) on strain.

The stress-strain curves for orthorhombic Li_7Sn_2 and cubic $Li_{17}Sn_4$ phases are given in Figs. 1(g) and 1(h). It is shown that both Li_7Sn_2 and $Li_{17}Sn_4$ exhibit strong stress responses in the principal symmetry crystallographic directions with the peak stress between 1–9 GPa and 2–6 GPa, respectively. The highest tensile stress of Li_7Sn_2 is 8.33 GPa in the [001] direction, which is higher than that (5.58 GPa) of $Li_{17}Sn_4$ in the [110] direction. Both of their weakest tensile directions are along the [100] direction, indicating that Li_7Sn_2 and $Li_{17}Sn_4$ could fracture in the [100] direction with a tensile strength of 1.27 and 2.81 GPa, respectively. Compared to the lowest tensile strength of Sn, these Li–Sn alloys are obviously weakened. On the other hand, the Li contents in Li–Sn alloys have an important influence on their mechanical properties. Figure 3 illustrates the tensile strength of alloy phases with respect to the Li fraction y of the alloy. Here, the Li fraction y is defined as the ratio of the Li atoms (x) to the total number of atoms in Li_xSn alloys, i.e., $y = x/(1 + x)$. As listed in TABLE I, all the alloy phases can be explored by the Li fraction y ranging from 0 (Sn) to 1 (Li). Generally speaking, the strength of a material can be approximately estimated as $E/10$, where E is Young's modulus.[16] To assess the validity of first-principles calculations, the values of $E/10$ for Li–Sn alloys are also given in Fig. 3, where the values of E are taken from Ref. 7.

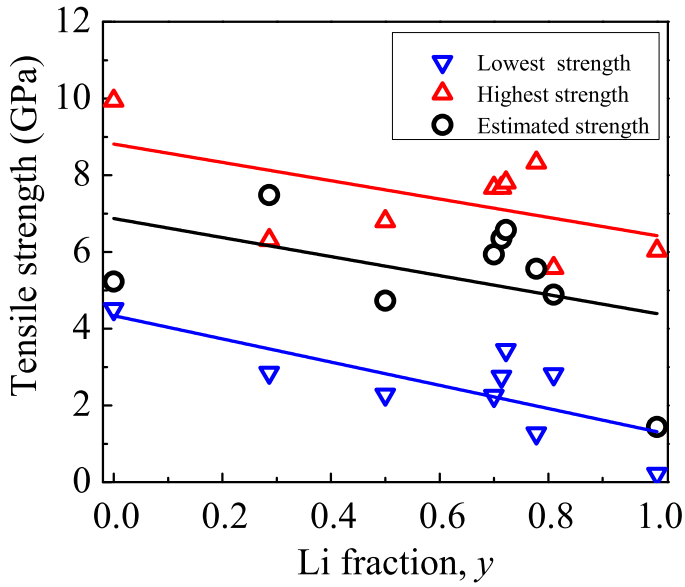

FIG. 3. The calculated highest and lowest tensile strengths, as well as the estimated strengths of $E/10$, for Li–Sn alloys versus the Li fraction y.

It is of interest to note that the estimated strengths are well consistent with our calculated results (see Fig. 3). The strengths of Li–Sn alloys decrease with the increase of Li-ion concentration and their lowest tensile strengths vary from 4.51 GPa (Sn) to 1.27 GPa (Li_7Sn_2). That is, the resistant ability of Li–Sn alloys to failure is weakened with increasing Li-ion concentrations. The gradually decreased tensile strengths of Li–Sn alloys make them more likely to suffer damage, which further leads to fracture and pulverization of electrode materials during lithiation. The similar trend has been discovered in their elastic properties, where bulk, shear and Young's moduli of isotropic Li_xSn alloys decrease almost linearly with the increase of Li-ion concentration.[7] This is because the Sn–Sn covalent bonds are gradually replaced by the weaker Li–Sn and Li–Li bonds with continuation of lithiation process.[17] The influence of bond change on the alloys is that the average strength of constituent chemical bonds is weakened, resulting in a weakened tendency of their resistant ability to deformation with the increase of Li concentration. Thus, it is the average weakened bond strength that results in the almost linearly decreased mechanical properties in elastic and large strain of Li–Sn alloys.

IV. CONCLUSIONS

Based on the density functional theory calculations, we have systematically studied the Li concentration-dependent mechanical properties of Li–Sn alloys. The results show that the tensile strengths of Li–Sn alloys decrease with the increase of Li-ion concentration, demonstrating their gradually weakened resistance to failure. The results provide a deep understanding on the mechanical properties of Li–Sn alloys in different lithiation states and give an explanation on fracture and pulverization of electrode materials during lithiation from the perspective of tensile strength. Furthermore, these strength data will be helpful in selecting an optimal structure of Sn anode materials and predicting their fracture during lithiation and delithiation processes.

ACKNOWLEDGMENTS

This work was supported by the National Natural Science Foundation of China (Grant Nos. 11372267, 11402086 and 11472141), and the National High Technology Research and Development Program of China (863 Program) (Grant No. 2013AA032502). Computations were supported by

resources provided by the Pawsey Supercomputing Center with funding from the Australian Government and the Government of Western Australia.

[1] B. Luo and L. Zhi, Energy Environ. Sci. **8**, 456-477 (2015).
[2] N. Alias and A. A. Mohamad, J. Power Sources **274**, 237-251 (2015).
[3] S. Iwamura, H. Nishihara, Y. Ono, H. Morito, H. Yamane, H. Nara, T. Osaka, and T. Kyotani, Sci. Rep. **5**, 8085-8093 (2015).
[4] C. Wu, J. Maier, and Y. Yu, Adv. Func. Mater. **25**, 3488-3496 (2015).
[5] A. Kushima, J. Y. Huang, and J. Li, ACS Nano **6**, 9425-9432 (2012).
[6] J. Wang, F. Fan, Y. Liu, K. L. Jungjohann, S. W. Lee, S. X. Mao, X. Liu, and T. Zhu, J. Electrochem. Soc. **161**, F3019-F3024 (2014).
[7] P. Zhang, Z. Ma, Y. Wang, Y. Zou, W. Lei, Y. Pan, and C. Lu, RSC Adv. **5**, 36022-36029 (2015).
[8] C. Y. Chou, H. Kim, and G. S. Hwang, J. Phys. Chem. C **115**, 20018-20026 (2011).
[9] C. Q. Sun, Prog. Solid State Chem. **35**, 1-159 (2007).
[10] M. Gu, C. Q. Sun, Z. Chen, T. A. Yeung, S. Li, C. Tan, and V. Nosik, Phys. Rev. B **75**, 125403-125412 (2007).
[11] D. Roundy, C. Krenn, M. L. Cohen, and J. Morris, Jr., Philos. Mag. A **81**, 1725-1747 (2001).
[12] G. Kresse and J. Furthmüller, Phys. Rev. B **54**, 11169-11186 (1996).
[13] D. M. Ceperley and B. Alder, Phys. Rev. Lett. **45**, 566-569 (1980).
[14] G. Kresse and D. Joubert, Phys. Rev. B **59**, 1758-1775 (1999).
[15] H. J. Monkhorst and J. D. Pack, Phys. Rev. B **13**, 5188-5192 (1976).
[16] Y. Zhou, L. Yang, and Y. Huang, *Micro- and Macromechanical Properties of Materials* (CRC Press, 2013).
[17] K. Li, H. Xie, J. Liu, Z. Ma, Y. Zhou, and D. Xue, Phys. Chem. Chem. Phys. **15**, 17658-17663 (2013).
[18] C. S. Barrett and T. B. Massalski, *Structure of Metals* (McGraw-Hill, New York, 1966).
[19] D. Hansen and L. Chang, Acta Crystallogr. **25**, 2392-2395 (1969).
[20] W. Müller and H. Schäfer, Z. Naturforsch B **28**, 246-248 (1973).
[21] W. Müller, Z. Naturforsch B **29**, 304-307 (1974).
[22] U. Frank, W. Müller, and H. Schäfer, Z. Naturforsch B **30**, 1-5 (1975).
[23] U. Frank and W. Müller, Z. Naturforsch B **30**, 316-322 (1975).
[24] U. Frank, W. Müller, and H. Schäfer, Z. Naturforsch B **30**, 6-9 (1975).
[25] C. Lupu, J.-G. Mao, J. W. Rabalais, A. M. Guloy, and J. W. Richardson, Inorg. Chem. **42**, 3765-3771 (2003).
[26] J. I. Gersten and F. W. Smith, *The physics and chemistry of materials* (Wiley, New York, 2001).